Cell. Mol. Life Sci. (2012) 69:1889–1901
DOI 10.1007/s00018-011-0908-y

Cellular and Molecular Life Sciences

RESEARCH ARTICLE

Geometry sensing by dendritic cells dictates spatial organization and PGE_2-induced dissolution of podosomes

Koen van den Dries · Suzanne F. G. van Helden · Joost te Riet · Ruth Diez-Ahedo · Carlo Manzo · Machteld M. Oud · Frank N. van Leeuwen · Roland Brock · Maria F. Garcia-Parajo · Alessandra Cambi · Carl G. Figdor

Received: 27 May 2011 / Revised: 28 November 2011 / Accepted: 13 December 2011 / Published online: 28 December 2011

Abstract Assembly and disassembly of adhesion structures such as focal adhesions (FAs) and podosomes regulate cell adhesion and differentiation. On antigen-presenting dendritic cells (DCs), acquisition of a migratory and immunostimulatory phenotype depends on podosome dissolution by prostaglandin E_2 (PGE_2). Whereas the effects of physico-chemical and topographical cues have been extensively studied on FAs, little is known about how podosomes respond to these signals. Here, we show that, unlike for FAs, podosome formation is not controlled by substrate physico-chemical properties. We demonstrate that cell adhesion is the only prerequisite for podosome formation and that substrate availability dictates podosome density. Interestingly, we show that DCs sense 3-dimensional (3-D) geometry by aligning podosomes along the edges of 3-D micropatterned surfaces. Finally, whereas on a 2-dimensional (2-D) surface PGE_2 causes a rapid increase in activated RhoA levels leading to fast podosome dissolution, 3-D geometric cues prevent PGE_2-mediated RhoA activation resulting in impaired podosome dissolution even after prolonged stimulation. Our findings indicate that 2-D

Koen van den Dries and Suzanne F.G. van Helden contributed equally to this work.

Electronic supplementary material The online version of this article (doi:10.1007/s00018-011-0908-y) contains supplementary material, which is available to authorized users.

K. van den Dries · S. F. G. van Helden · J. t. Riet · M. M. Oud · F. N. van Leeuwen · A. Cambi · C. G. Figdor (✉)
Department of Tumor Immunology, Nijmegen Centre for Molecular Life Sciences, Radboud University Nijmegen Medical Centre, P.O. Box 9101, 6500 HB Nijmegen, The Netherlands
e-mail: c.figdor@ncmls.ru.nl

R. Diez-Ahedo
BioNanoPhotonics Group, IBEC-Institute for Bioengineering of Catalonia and CIBER-bbn, Baldiri Reixac 15-21, 08028 Barcelona, Spain

R. Brock
Department of Biochemistry, Nijmegen Centre for Molecular Life Sciences, Radboud University Nijmegen Medical Centre, 6500 HB, Nijmegen, The Netherlands

Present Address:
S. F. G. van Helden
Department of Molecular Cell Biology, Sanquin Research and Landsteiner Laboratory, Academic Medical Centre, University of Amsterdam, 1066 CX Amsterdam, The Netherlands

Present Address:
F. N. van Leeuwen
Laboratory of Pediatric Oncology, Nijmegen Centre for Molecular Life Sciences, Radboud University Nijmegen Medical Centre, 6500 HB Nijmegen, The Netherlands

C. Manzo · M. F. Garcia-Parajo
ICFO-Institut de Ciencies Fotoniques, Mediterranean Technology Park, 08860 Barcelona, Spain

M. F. Garcia-Parajo
ICREA-Institució Catalana de Recerca i Estudis Avançats, 08010, Barcelona, Spain

and 3-D geometric cues control the spatial organization of podosomes. More importantly, our studies demonstrate the importance of substrate dimensionality in regulating podosome dissolution and suggest that substrate dimensionality plays an important role in controlling DC activation, a key process in initiating immune responses.

Keywords Mechanosensitivity · Podosomes · Dendritic cell · Adhesion

Abbreviations

ECM	Extracellular matrix
2-D	2-Dimensional
3-D	3-Dimensional
FA	Focal adhesion
DC	Dendritic cell
iDC	Immature dendritic cell
PGE_2	Prostaglandin E_2
PS	Polystyrene
PEN	Polyethylene naphtalate
PMMA	Poly(methyl methacrylate)
PLL	Poly-L-lysine
PEG	Poly(ethylene glycol)
NND	Nearest neighbour distance
NNA	Nearest neighbour angle

Introduction

Living cells are continuously exposed to a large variety of exogenous signals. They have the ability to sense chemicals, in the form of soluble factors, extracellular matrix (ECM), and receptors on adjacent cells. Similarly, they can respond to physical cues, such as substrate rigidity and geometric constraints [1]. Both chemical and physical signals can jointly be presented in two and three dimensions, adding another level of complexity to the array of environmental signals that influences a cell. Through its extensive sensory machinery, a cell integrates these signals to direct key processes such as adhesion, growth, and differentiation [2–4]. Depending on outside–in as well as inside–out signaling, integrin-based adhesion sites are thought to play a major role in both the perception of external stimuli and the execution of the cellular response [5–7].

To mimic the cellular biochemical microenvironment, cells are frequently seeded on substrates coated with different ECM components or recombinant receptor proteins. Physical parameters usually involve altered substrate stiffness and ligand spatial organization in 2-dimensional (2-D) conditions [8, 9]. Progress in micro- and nanotechnology now allows the addition of the third dimension to the microenvironment, thus enabling a much closer mimicry of the in vivo situation. Evidence is accumulating that substrate dimensionality plays an important role in controlling the assembly of the actin cytoskeleton and its adhesive structures [10, 11].

Focal adhesions (FAs) and podosomes are adhesion structures which represent hotspots of integrins, stretch-activated ion channels, and cytosolic proteins like myosin and talin [12]. Each of these proteins plays an essential role in translating both chemical and physical information into biochemical downstream signals that regulate cell adhesion and migration [13–16]. FAs are relatively stable tangential structures connected to actin stress fibers and are present in a broad range of cell types [17]. By contrast, podosomes are highly dynamic dot-shaped adhesion complexes of approximately a micron that have first been identified in Src-transformed fibroblasts [18–20]. They share many cytoskeletal components with FAs, such as paxillin, talin, and vinculin, but they also contain characteristic molecules such as cortactin, dynamin2, and Tks4/5 [12, 21–23]. Podosomes are observed in smooth muscle cells, activated endothelial cells, and cells of myeloid origin, including osteoclasts, monocytes, macrophages, and dendritic cells (DCs) [24, 25].

Dendritic cells, as key regulators of both the innate and adaptive immune response, migrate over long distances through tissues, thereby encountering a large range of distinct extracellular microenvironments. Tissue-resident immature DCs (iDCs) sample peripheral tissues for invading pathogens. Upon encountering an antigen, iDCs become activated to turn into mature DCs (mDCs) and migrate to a regional lymph node, where they present the antigen to T cells, thereby initiating an immune response [26, 27]. Podosomes have been shown to play an important role in both the adhesive and migratory properties of DCs. iDCs form large numbers of podosomes and exhibit an adhesive phenotype, while the maturation of DCs is accompanied by the dissolution of podosomes, which is required to accommodate the high-speed amoeboid migration observed in mDCs [28, 29]. We have shown before that prostaglandin E_2 (PGE_2) plays a critical role in the dissolution of podosomes and that the loss of podosomes during DC maturation is essential for full activation of immune responses [30].

Thus far, most studies on environmental signals and cell adhesion have focused on FAs and showed that various exogenous signals affect the formation, maturation and the spatial distribution of FAs [31–34]. Although podosomes are also likely to be affected by environmental signals, this has never been thoroughly addressed. Recently, Collin et al. [35, 36] showed that podosomes act as mechanosensors by responding to substrate rigidity and applied stress. In addition, it has been shown that different biomimetic calcite crystals are able to influence podosome behavior in osteoclasts [37, 38]. However, how environmental signals precisely control the formation and spatial

organization of podosomes is still largely unknown. Moreover, a systematic investigation of podosome behavior to different chemical and geometric environmental signals is lacking.

Here, we investigated how differential chemical and geometric signals affect the spatial organization and dissolution of podosomes in human DCs. We show that an adhesive substrate is a prerequisite for podosome formation, whereas the chemical nature of the substrate is not critical. Furthermore, we demonstrate that DCs respond to 3-D geometric cues by rearranging podosome spatial organization. Finally, we present evidence that 3-D geometric cues inhibit podosome dissolution, underlining the relevance of substrate dimensionality for cell adhesion and behavior.

Materials and methods

Chemicals, antibodies and bacteria

The following antibodies or appropriate isotype controls were used: rIgG1-FITC (BD Bioscience Pharmingen, San Diego, CA, USA), anti-vinculin (Sigma, St. Louis, MO, USA), anti-HLA-DR/DP (Q5/13), anti-CD80 (all BD Biosciences, Mountain View, CA, USA), anti-CD83 (Beckman Coulter, Mijdrecht, The Netherlands), anti-CCR7 (R&D Systems, Minneapolis, MN, USA), Alexa Fluor 488-labeled secondary antibody (GaM) and Texas Red-conjugated phalloidin were from Molecular Probes (Molecular Probes, Leiden, The Netherlands). The following chemicals were used: fibronectin (Roche, Mannheim, Germany), gelatin, laminin and poly-L-lysine (PLL) (Sigma), polytetrafluoroethylene (Teflon), polystyrene (PS), polyethylene naphthalate (PEN), and impact modified poly(methyl methacrylate) (PMMA) (Goodfellow, Bad Nauheim, Germany). Hydrogels are p-slides from Nexterion (Schott, Mainz, Germany). PGE_2 is used at 10 μg/ml (Sigma). *N. meningitides* H44/76 was isolated from a patient with invasive meningococcal disease (kindly provided by Dr. P van der Ley, Laboratory of Vaccine Research, Netherlands Vaccine Institute, Bilthoven, The Netherlands). *S. aureus* was obtained from the American Type Culture Collection (ATCC 43300). All bacteria were heat-killed and used at multiplicity of infection (MOI) 20. For FITC-labeling, bacteria were washed in PBS and incubated in 0.5 mg/ml FITC for 60 min. FITC-labeled bacteria were thoroughly washed and stored in PBS at −20°C.

Preparation of human DCs

Dendritic cells were generated from PBMCs as described previously [39]. Monocytes were derived from buffy coats. Plastic-adherent monocytes were cultured in RPMI 1640 medium (Gibco; Life Technologies, Breda, The Netherlands) supplemented with 10% (v/v) FCS (Greiner, Kremsmuenster, Austria), IL-4 (500 U/ml) and GM-CSF (800 U/ml). Immature DCs were harvested on day 6 and the expression of MHC class I/II, costimulatory molecules and DC-specific markers were measured by flow cytometry (data not shown).

Substrate preparation

Coverslips were coated with fibronectin (20 μg/ml) in PBS for 1 h at 37°C, gelatin (0.01% w/v) in PBS for 30 min at 37°C, laminin (20 μg/ml) in PBS for 1 h at 37°C, PLL (100 μg/ml) in PBS for 30 min at 37°C or left untreated. The substrates with different heights of Teflon, PS, PEN, and PMMA were made with hot embossing.

Hydrogel spotting

Drops (0.5 ml) of PBS with fibronectin (200 μg/ml) were spotted on hydrogels. The spotted hydrogels were washed with PBS and 4×10^4 DCs in 100 μl RPMI 1640 medium with cytokines were seeded.

Microcontact printing

A silicon wafer was made with photolithography. PDMS Sylgard 184 silicone elastomer was mixed with a cross-linking agent containing a Pt-catalysator (both from Dow Corning, Midland, MI, USA) at a ratio of 10:1. Gas bubbles were removed in the exsiccator for $\approx$30 min. The wafer was placed with the structured surface faced up and a few ml of the PDMS were poured onto it. The mixture was degassed again. Polymerization was achieved during incubation at 60–65°C for approximately 20 h. After polymerization, the stamp was peeled off the wafer. The stamps were incubated with fibronectin (100 μg/ml)/rIgG1-FITC (5 μg/ml) for 1 h at RT in the dark. The solution was removed and the stamp was washed with milliQ and dried with oil-free N_2 using waferguard pistol (Millipore, Billerica, MA, USA). The stamp was placed on the hydrogel and removed again. The printed area of the hydrogel was washed with 200 μl PBS and 9×10^4 DCs in 150 μl RPMI 1640 with cytokines were seeded.

Atomic force microscopy

The substrate topography was quantitatively evaluated using atomic force microscopy (AFM; Dimension 3,100; Veeco, Santa Barbara, CA, USA). Tapping in ambient air was performed with two types of cantilevers. The topography of the 3-D micropatterned substrates was determined

with a 118-μm-long, high aspect ratio silicon cantilever (NW-AR5T-NCHR; NanoWorld, Wetzlar, Germany). The patterns of Fig. S3C in the supplementary material were analyzed with a 100-μm-long, gold-coated silicon cantilever (NSG-10; NT-MDT, Moscow, Russia). Both type of cantilevers have a nominal radius of curvature of the AFM probe tip of less than 10 nm. Height images of each sample were captured in air at 50% humidity at tapping frequencies of 271 and 261 kHz for the NSG-10 and NW-AR5T-NHCR cantilevers, respectively. The analyzed fields were scanned at scan rates between 0.2 and 0.8 Hz and with 512 × 256 or 512 × 512 scanning resolution. Nanoscope imaging software (v.6.13r1, Veeco) was used to analyze the images.

Fluorescent microscopy

Dendritic cells were seeded on substrates and left to adhere for 16 h. The cells were fixed in 3.7% (w/v) formaldehyde in PBS for 10 min. Cells were permeabilized in 0.1% (v/v) Triton X-100 in PBS for 5 min and blocked with 2% (w/v) BSA in PBS. The cells were incubated with primary Ab for 1 h. Cells were subsequently incubated with Alexa Fluor 488-labeled secondary antibodies for 45 min. Subsequently, cells were incubated with Texas Red-conjugated phalloidin for 30 min. Images were collected on a Leica DMRA fluorescence microscope with a ×63 PL APO 1.3 NA oil immersion lens (or a ×40 PL FLUOTAR 1.0 NA oil immersion lens for overview images) and a COHU high performance integrating CCD camera (COHU, San Diego, CA, USA). Confocal images were collected on a Zeiss LSM 510 microscope, using a PlanApochromatic 63 × 1.4 oil immersion DIC lens (Carl Zeiss GmbH, Jena, Germany). Pictures were analyzed with Leica Qfluoro v.V1.2.0 (Leica) and ImageJ 1.40 (http://rsbweb.nih.gov/ij/) software.

RhoA activity assay

To measure RhoA GTP levels, cells were seeded on a flat surface or on a 3-D micropatterned surface and allowed to adhere for 16 h. Subsequently, cells were stimulated for 1 min with 10 μg/ml PGE_2 or left untreated. RhoA activity was measured by a luminometry based G-LISA assay (Tebu-Bio, Heerhugowaard, The Netherlands), according to the manufacturer's guidelines. The G-LISA assay reports levels of active RhoA normalized by protein input levels. Levels of luminescence were detected using a Victor 3 luminometer (PerkinElmer).

Statistical analysis

ANOVA test or Student's t test was used for statistical analysis. Significant differences were determined at $p < 0.05$.

Results

Podosome formation does not depend on physico-chemical properties of the substrate

Focal adhesions and podosomes are the two main surface-sensing complexes formed by DCs (Fig. 1a). To investigate how substrate physico-chemical properties influence the formation of FAs and podosomes, DCs were seeded on 2-D surfaces with decreasing hydrophobicity: Teflon, PS, PEN, and PMMA.

Although hydrophobic surfaces are generally considered non-permissive for cell adherence, DCs readily adhered and developed podosomes on all of the tested surfaces with a constant number of podosomes per cell (Fig. 1b, c). Interestingly, while the number of podosome-bearing cells was comparable in all conditions, the DCs responded to the hydrophilic surfaces PEN and PMMA by forming significantly fewer FAs (Fig. 1d). Furthermore, podosome formation was not affected by the molecular nature of the substrate as we observed similar podosome formation on different integrin ligands (fibronectin, gelatin, and laminin) as well as on the unspecific PLL coating and uncoated glass (Fig. S1 in supplementary material). For all conditions, podosome formation was already observed within 1 h after seeding (data not shown). More importantly, the presence or absence of serum in the medium did not influence the observed adhesive behavior of DCs (data not shown).

Together, these results indicate that the formation of podosomes in DCs does not depend on the physico-chemical properties of the surface nor on the chemical composition of the coating and suggest that podosomes are less discriminative in sensing physico-chemical cues from their microenvironment than FAs.

2-D geometric constraints of adhesion permissive substrate directs podosome spatial organization

To show that cell adhesion is the only prerequisite for the formation of podosomes, we investigated podosome formation on a surface that is non-permissive for cell adhesion. To this end, we used a thin-film hydrogel-coated surface. In our case, the hydrogel consisted of a poly(ethylene glycol) (PEG) coating which is generally used for protein microarrays [40]. Hydrogels are considered non-permissive for cell adhesion because of their very low unspecific binding properties [41]. Indeed, DCs did not adhere on these hydrogels (Fig. 2a). However, when these hydrogels were coated with fibronectin, DCs readily adhered and formed podosomes (Fig. 2a). Intriguingly, podosome formation did not depend on fibronectin-mediated activation of integrins, since DCs adhered equally well to, and formed podosomes on, PLL-coated hydrogels (data not shown).

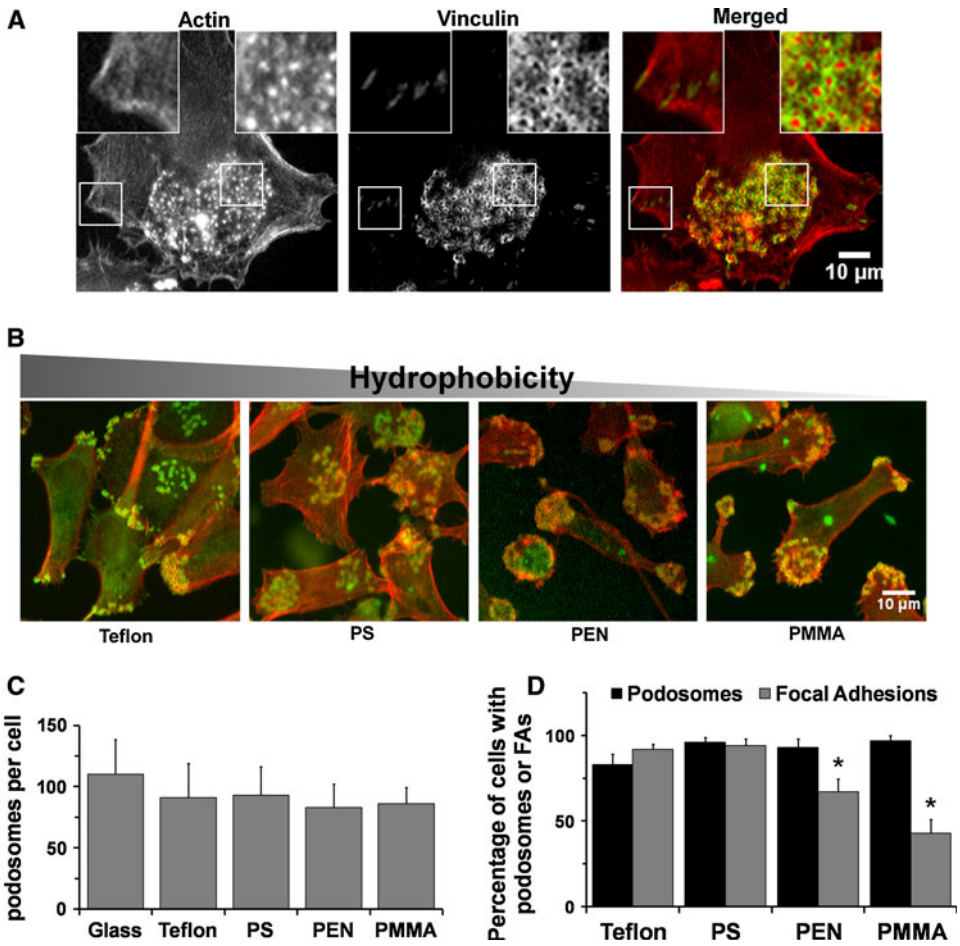

Fig. 1 Podosome formation is not influenced by substrate physico-chemical properties. **a** DCs seeded on glass form two types of adhesion structures. The cells were fixed and stained with phalloidin–Texas Red and an anti-vinculin mAb to visualize actin (*red*) and vinculin (*green*), respectively. Podosomes (*right insert*) can be seen as small circular structures, whereas FAs (*left insert*) are tangential. **b** Cells were seeded on Teflon, PS, PEN, and PMMA with Teflon being most hydrophobic and PMMA most hydrophilic. Cells were fixed and stained with phalloidin–Texas Red and an anti-vinculin mAb to visualize actin (*red*) and vinculin (*green*), respectively. Representative pictures are depicted. **c** Quantification of the number of podosomes per DC on surfaces with different hydrophobicity. Podosomes were counted in 15 cells in two independent experiments. *Bars* mean ± SD. **d** The number of cells displaying podosomes or FAs was counted in seven images per condition. *Asterisks* significant differences from Teflon ($p < 0.05$). *Bars* mean ± SEM

Next, we investigated how 2-D surface geometry dictates the formation and spatial organization of podosomes by spotting a 2-D micropattern of fibronectin on the hydrogels. When seeded, DCs covered long distances of non-coated hydrogel. However, cells were able to discriminate between adhesive and non-adhesive areas by selectively forming podosomes on the adhesive spots (Fig. 2b; Fig. S2 in supplementary material). We determined if the size of the adhesive spots affected podosome spatial rearrangement, and quantified the number of podosome clusters with respect to the size of fibronectin spots (diameter ranging from 5 to 20 µm). As expected, the number of podosome clusters per cell inversely correlated with spot size (Fig. 2c), mainly due to the fact that DCs spanned fewer spots when seeded on large 20-µm spots in comparison with small 5-µm spots (Fig. S2D in supplementary material). In addition, the number of podosomes formed on the spots correlated directly with the spot size (Fig. 2d). Intriguingly, although the spatial organization of podosomes is dictated by the spots, the number of podosomes per cell remained remarkably stable (Fig. 2e). This resulted in a higher podosome density on the 5-µm spots compared to the 20-µm spots (Fig. 2d). The local podosome density found on the 5-µm spots is ≈ 0.8 podosomes/µm^2. With a podosome of approximately 0.78 µm^2 (radius ≈ 0.5 µm), the packaging of podosomes on the minimal amount of available substrate is almost maximal. In contrast, the density on the large 20-µm spots is comparable to the density on normal flat substrates (≈ 0.2 podosomes/µm^2). Altogether, these findings indicate that cell adhesion, irrespective of the exact chemical nature of the adhesive surface, dictates podosome formation and

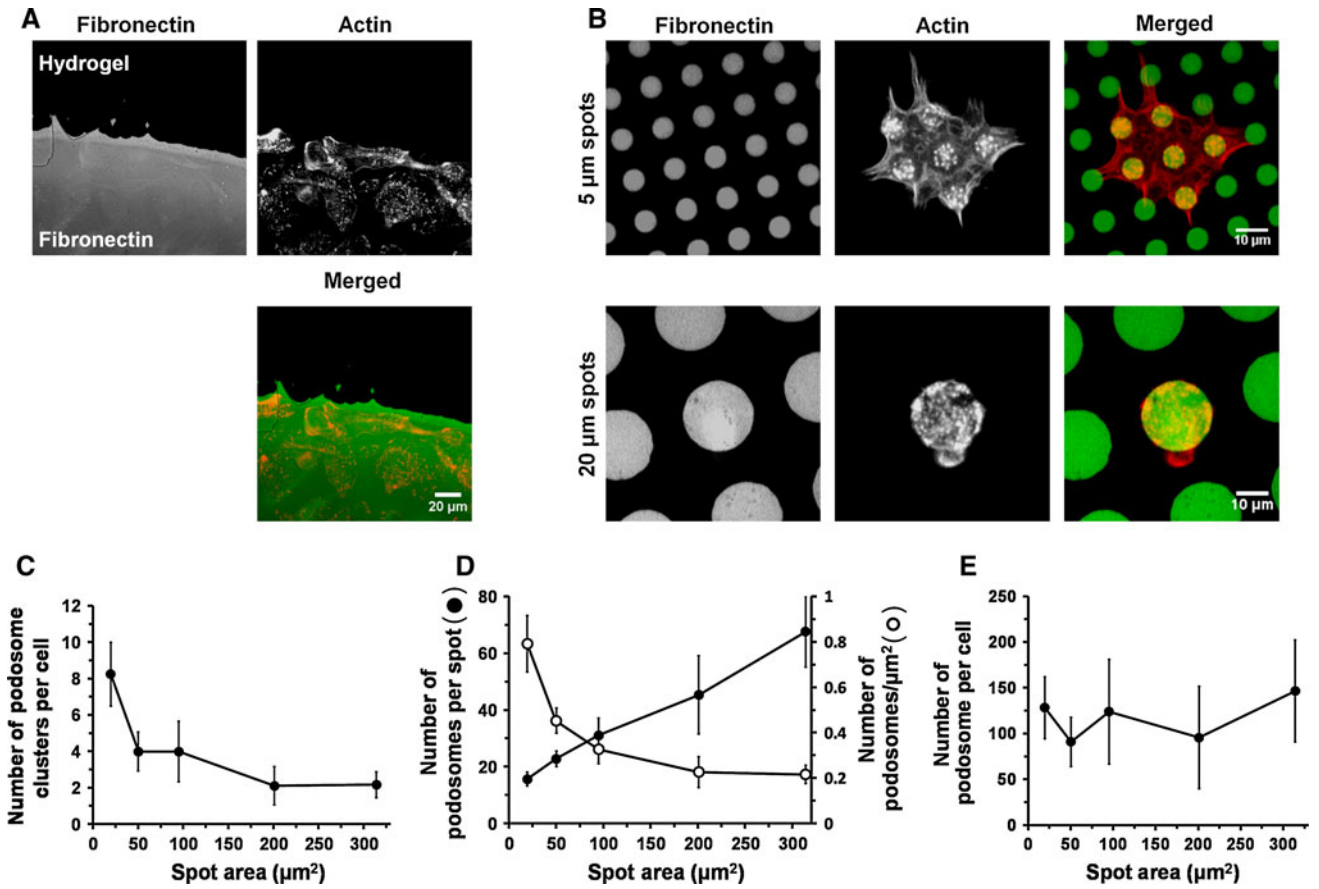

Fig. 2 Podosomes formation is exclusively dependent on cell adhesion. **a** Hydrogels were coated with fibronectin mixed with rIgG-FITC (*green*) for visualization. DCs were seeded on the hydrogel and stained with phalloidin–Texas Red to visualize actin (*red*). Cells were found to adhere specifically to the fibronectin-coated areas. Representative image is depicted. Coating with rIgG-FITC alone was not sufficient for DC adherence (not shown). **b** Cells were seeded on fibronectin/rIgG1-FITC (*green*) printed hydrogel and fixed and stained with phalloidin–Texas Red to visualize actin (*red*). Representative images of cells seeded on 5- and 20-µm dots are depicted in the *upper* and *lower panels*, respectively. The distance between the spots is 7.5 and 10 µm for the 5- and 20-µm spots, respectively. **c** The number of podosome clusters per cell was quantified for the different sized dots and spacing. **d** Quantification of the number of podosomes per spot and the podosome density on the different sized spots. **e** Quantification of the number of podosomes per cell on the different sized spots. Spots with diameters of 5, 8, 11 16 and 20 µm were used for analysis. All quantifications include at least 15 cells per single spot size and graphs represent mean ± SD

that 2-D geometric constraints of the adhesive substrate direct local podosome density in DCs.

3-D geometric cues control podosome spatial organization

It is well established that the actin cytoskeleton responds differently to 2-D versus 3-D environmental signals. So far, our data clearly showed that 2-D environmental cues do not influence the formation of podosomes although podosome spatial organization is affected. In order to investigate whether podosome formation is influenced by 3-D geometric cues, DCs were seeded on various 3-D micropatterned substrates, with a height of 1 µm and a width ranging from 2 to 20 µm (Fig. 3a), as confirmed by atomic force microscopy (data not shown). When seeded on these 3-D micropatterned substrates, DCs oriented parallel to the direction of the patterns. Surprisingly, podosomes were predominantly formed on the edge of the patterns (Fig. 3b). The magnified insets clearly show that, even in the aligned configuration, individual podosomes could still be identified. To quantify the degree of podosome alignment, we determined the angles of the nearest neighbor distance (NND) with respect to the *y* axis (Fig. S3A in supplementary material). On a flat surface, these nearest neighbor angles (NNA) were randomly distributed, whereas the micropatterned substrates clearly induced a polarization of the NNA towards 90° (Fig. 3c). Alignment of podosomes proved to be independent of surface hydrophobicity, as podosome alignment was also observed on PS, PEN, and PMMA 3-D micropatterned substrates (Fig. S3B).

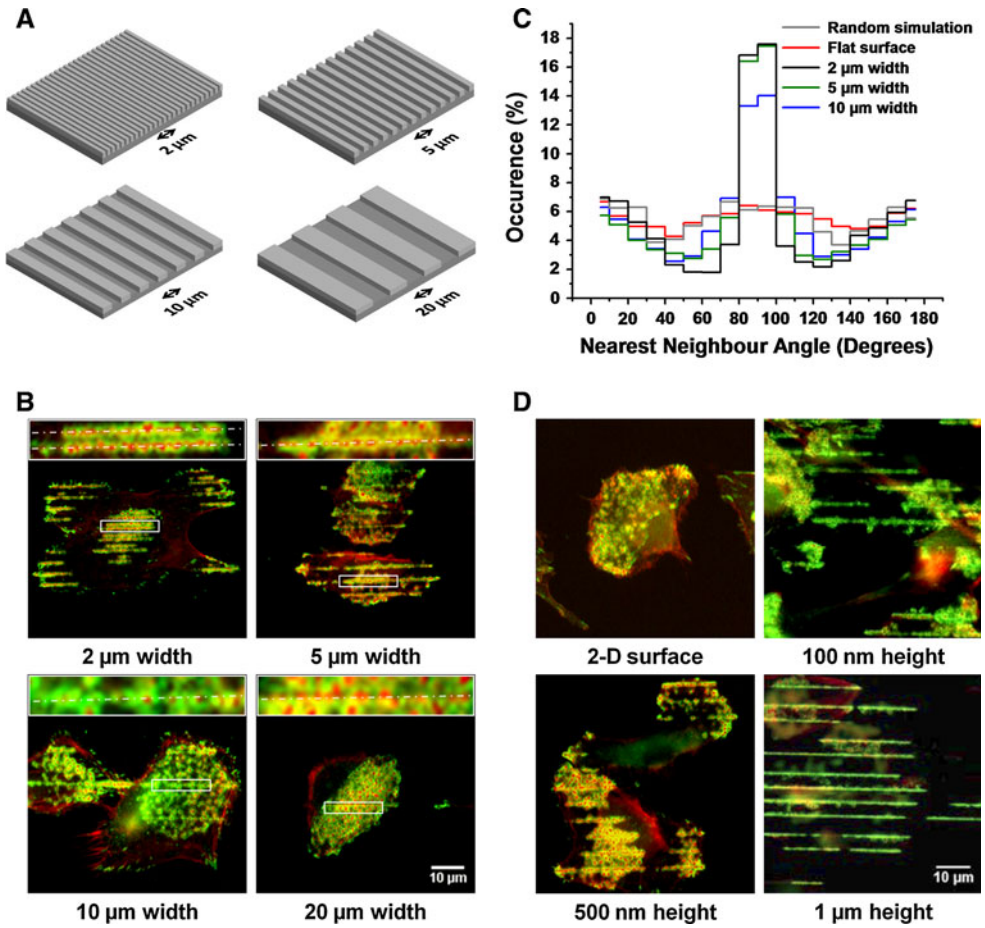

Fig. 3 Podosomes align along the edges of 3-D micropatterned substrates. **a** Schematic representation of the 3-D micropatterned substrates. 3-D micropatterns with widths of 2, 5, 10 and 20 µm and 1 µm height were fabricated. All 3-D micropatterns were fabricated such that the top and lower part had the same width. **b** DCs were seeded on 3-D micropatterned substrates with a height of 1 µm and widths of 2, 5, 10 and 20 µm. Cells were fixed and stained with phalloidin–Texas Red and an anti-vinculin mAb to visualize actin (*red*) and vinculin (*green*), respectively. The *dotted lines* in the *insets* indicate the position of the edges of the micropatterned substrate. Representative images are depicted. **c** The nearest neighbor angles (NNA) of podosomes (Fig. S3A in supplementary material) reveal the alignment of podosomes on the edges of 3-D patterns. The 2-µm 3-D micropattern induces a polarization of the NNA towards 90°. **d** DCs were seeded on a flat surface and on 3-D micropatterned substrates of 5 µm width and 100 nm, 500 nm and 1 µm height. Cells were fixed and stained with phalloidin–Texas Red and an anti-vinculin mAb to visualize actin (*red*) and vinculin (*green*), respectively. Representative images are depicted

Moreover, podosomes aligned always along the edges irrespective of the shape of the pattern (Fig. S3C). To address whether nanoscale changes in the substrate geometry also controlled podosome spatial organization, micro- and nanopatterned substrates with heights ranging from 100 nm to 1 µm were fabricated. Strikingly, DCs were still able to sense height differences as small as 100 nm by placing podosomes along the 90° edges (Fig. 3d). These results indicate that the spatial organization of podosomes is directed by substrate geometry, irrespective of the substrate physico-chemical properties. 3-D micropatterned substrates with a height as small as 100 nm affect the spatial organization of podosomes suggesting that the underlying mechanism is extremely sensitive for 3-D geometric cues.

Substrate dimensionality affects the spatial arrangement of podosomes

We observed that, on 2-D surfaces, DCs formed a remarkably constant number of podosomes, irrespective of substrate physico-chemical properties. Interestingly, we also found no differences in podosome number between flat and patterned surfaces (Fig. 4a). While, on 2-µm-wide micropatterns, all podosomes exclusively aligned on the edges of the patterns and no podosomes were detected on the flat areas, podosomes were detected on the flat areas when the distance between the edges became wider than 2 µm.

As the cell membrane folds around the edge of the micropatterned substrate, both an inward and an outward

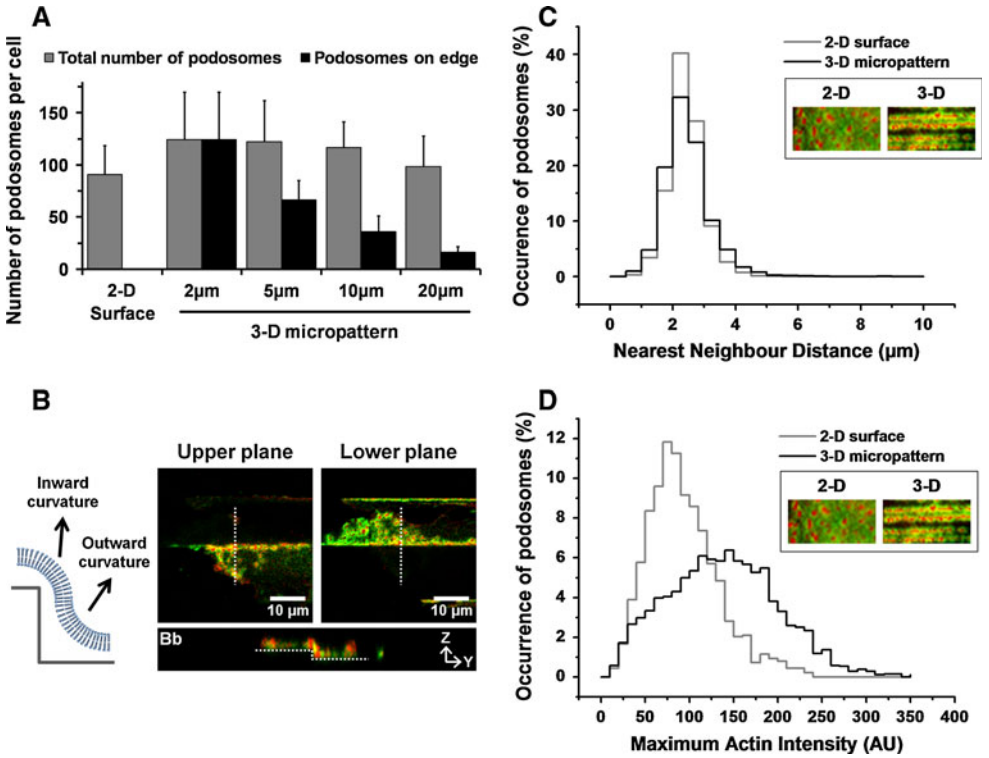

Fig. 4 3-D geometric cues influence podosome spatial organization and actin content. **a** Quantification of the number of podosomes per DC on 2-D and 3-D micropatterned substrates with widths of 2, 5, 10 and 20 μm together with the number of podosomes on the edges. Graphs represent mean ± SD of at least 20 cells per condition. **b** Inward and outward curvatures are created at the plasma membrane at the upper and lower edge of the 3-D micropattern. DCs were seeded on micropatterns with a height of 1 μm. Z-stacks were taken every 300 nm. Podosomes align on both the upper and the lower corner of the pattern. Shown are the lower and upper plane of the z-stack. The *white dashed line* represents the slice of the orthogonal view shown in *Bb*. **c** Nearest neighbor distance was determined for podosomes on 3-D micropatterns and 2-D surfaces. The average inter-podosomal distance on flat surfaces and patterns was 1.93 ± 0.54 μm ($n = 4{,}342$) and 1.91 ± 0.79 μm ($n = 6{,}177$), respectively ($p = 0.16$). **d** Cells were fixed and stained with phalloidin–Texas Red to visualize actin. The maximum Texas Red intensity on 3-D micropatterns and 2-D surfaces was 128 ± 62 ($n = 1{,}387$) and 83 ± 40 ($n = 2{,}791$), respectively ($p < 0.01$). *Insets* in (**c**) and (**d**) show podosomes on a flat 2-D surface and a 3-D micropattern. Podosomes are visualized by staining actin (*red*) and vinculin (*green*) with phalloidin–Texas Red and a vinculin-mAb, respectively

curvature are created (Fig. 4b). Plasma membrane bending is known to attract specific lipids and curvature-sensing proteins thereby creating local signaling platforms [42]. To investigate whether podosome alignment was mainly on the upper edge or the lower edge of the patterns, image stacks of 300 nm were taken of DCs on micropatterns with a height of 1 μm. Intriguingly, podosomes aligned on both the upper and the lower edges of the pattern (Fig. 4b). These results suggest that both a 90° inward and a 90° outward plasma membrane curvature creates a microenvironment favoring the nucleation of podosomes. This predominant formation of podosomes on the edge does not exclude the formation of podosomes on the flat parts of patterned substrates larger than 2 μm, suggesting a spatial signaling threshold for the nucleation of podosomes.

To further study the effect of 3-D geometric cues on the rearrangement of podosomes, we calculated the NND between podosomes on both the edges of the 3-D micropatterned substrates and 2-D surfaces. We found that inter-podosomal distance was not affected by the 3-D geometric cues as the average inter-podosomal distance on flat surfaces and the edges of 3-D micropatterns was 1.93 ± 0.54 μm ($n = 4{,}342$) and 1.91 ± 0.79 μm ($n = 6{,}177$), respectively ($p = 0.16$) (Fig. 4c). Instead, we noticed that the actin intensity, visualized by Texas Red-conjugated phalloidin, of each podosome core was significantly ($p < 0.01$) higher on the 3-D micropatterns compared to 2-D surfaces (Fig. 4d). This clearly indicates that the podosomes found on the edges have a higher actin content compared to podosomes on flat areas.

3-D geometric cues dictate PGE_2-mediated podosome dissolution and DC functionality

By regulating intracellular signaling pathways, matrix elasticity and tissue topography are known to affect cell fate decisions, such as cell cycle progression, differentiation, and apoptosis. Maturation of DCs is marked by

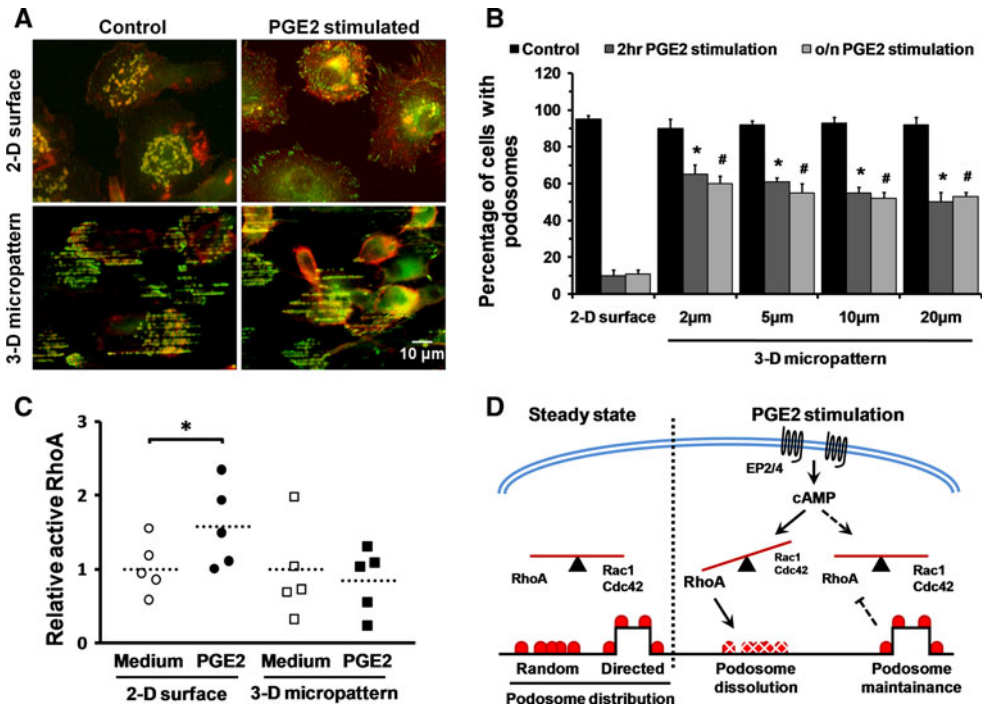

Fig. 5 3-D geometric cues inhibit PGE_2-mediated podosome dissolution. **a** iDCs were seeded on a 2-D surface and 3-D micropatterns and left untreated or stimulated with 10 μg/ml PGE_2. The cells were fixed and stained for phalloidin–Texas Red and an anti-vinculin mAb to visualize actin (*red*) and vinculin (*green*), respectively. Representative images are depicted. **b** The number of cells that contained podosomes was determined for seven images per condition. *Bars* mean ± SEM. $^{*}p < 0.05$ compared to 2 h PGE_2 stimulation on 2-D surface, $^{\#}p < 0.05$ compared to o/n PGE_2 stimulation on 2-D surface. **c** PGE_2-mediated activation of the small GTPase RhoA was measured on 2-D surfaces and 3-D micropatterned substrates by a luminometric G-LISA assay. Data were normalized to the active RhoA levels in the absence of PGE_2. *Dotted line* represents the average of five independent donors performed in duplicate ($^{*}p < 0.05$). **d** Schematic model of podosome distribution/dissolution on 2-D surfaces and 3-D micropatterned substrates. Whereas DCs form podosomes at random on 2-D surfaces, they specifically align their podosomes on the edges of 3-D micropatterned substrates. On 2-D surfaces, PGE_2 causes a rapid increase in RhoA activity leading to global podosome dissolution. In contrast, signals derived from signaling platforms induced by the 3-D micropatterns are able to prevent increased RhoA activity and thereby podosome dissolution

profound cytoskeletal alterations resulting in a switch from an adhesive to a highly migratory phenotype. For iDCs seeded on flat surfaces, we have shown before that binding of PGE_2 to the prostaglandin receptors EP_2 and EP_4 results in rapid podosome dissolution in iDCs, one of the first steps towards a fully mature DC phenotype [43]. To investigate whether DC signaling is influenced by substrate geometry, we stimulated iDCs, either on 2-D or 3-D micropatterned substrates, with PGE_2. Consistent with our prior results, after 2 h stimulation with PGE_2, podosomes on DCs seeded on 2-D surfaces almost completely dissolved (Fig. 5a). Strikingly, podosome dissolution became significantly impaired on the 3-D micropatterned substrates (Fig. 5a). Even prolonged stimulation with PGE_2 did not result in podosome dissolution on these 3-D micropatterned substrates (Fig. 5b). To investigate whether DC functionality is influenced by substrate geometry, we first determined whether phagocytic capacity, associated with the presence of podosomes [44], is influenced by 3-D micropatterned substrates. For this purpose, iDCs, either seeded on 3-D micropatterns or flat 2-D surfaces, were incubated with Gram-positive and Gram-negative bacteria, which we have shown before to be internalized equally effectively by iDCs [30]. Interestingly, we found that the internalization of both Gram-positive and Gram-negative bacteria was enhanced by iDCs seeded on 3-D micropatterned substrates (Figure S4A in supplementary material). The percentage of positive cells and the amount of internalized bacteria were found to be higher compared to 2-D substrates. Next, we investigated the differentiation status of iDCs seeded on 3-D micropatterned substrates for 24 h. As expected, when seeded on 2-D surfaces, iDCs express low levels of the costimulatory molecules CD80 and CD83 and the chemokine receptor CCR7, and they express high levels of MHC class II (Fig. S4B in supplementary material). Interestingly, while the surface expression levels of CD80, CD83, and CCR7 were unaffected on 3-D micropatterns, MHC class II molecules were expressed at even higher levels (Fig. S4B in supplementary material). Altogether, these results indicate that substrate dimensionality plays a key role in regulating the adhesive as well as the immunomodulatory properties of iDCs.

We have previously demonstrated that PGE_2-induced podosome dissolution in DCs is a result of cAMP-mediated increased activation of the small GTPase RhoA [43]. To further clarify the mechanism of reduced PGE_2-induced podosome dissolution on 3-D micropatterns, we studied the effect of geometric cues on RhoA activation. We measured activated RhoA levels on 2-D surfaces and 3-D micropatterned substrates (Fig. 5c). In the absence of PGE_2, no differences were observed in active RhoA levels between the 2-D surfaces and the 3-D micropatterned substrates. As expected, we detected increased RhoA activity on the 2-D surfaces after the addition of PGE_2. Remarkably, the 3-D micropatterns prevented the PGE_2-induced RhoA activation, clearly indicating that 3-D geometric cues are able to alter the activation of Rho GTPases, thus preventing podosome dissolution.

Discussion

In this study, we investigated how geometry sensing by human monocyte-derived DCs affects the spatial organization and PGE_2-induced dissolution of podosomes. We demonstrated that, unlike for FAs, substrate chemical properties do not affect podosome formation. By microcontact printing, we found that it is mainly the spatial organization of the adhesion permissive substrate that directs podosome distribution in DCs. Remarkably, the podosome number per cell was constant, even for adhesive spots of different size, meaning that the cells adjusted their podosome density depending on the substrate area. In addition, we showed that DCs respond to 3-D geometric cues by aligning their podosomes on the edges of 3-D micropatterned substrates. Finally, these 3-D geometric cues were able to overrule the PGE_2-induced signals, which on flat surfaces normally lead to podosome dissolution, suggesting that sensing of extracellular geometric cues can directly affect DC adhesion and thereby migration.

It is well known that both physico-chemical properties, e.g., hydrophobicity, and the chemical nature of the microenvironment can influence cellular adhesion. Whereas hydrophobic surfaces are generally less permissive for cell adhesion in comparison to hydrophilic surfaces [45–51], we show here that DCs adhere to and form podosomes on surfaces with a wide range of hydrophobicity. In contrast, the formation of FAs is significantly inhibited by hydrophilic surfaces. Furthermore, we observed that podosome formation is not influenced by the type of ECM coating. Altogether, these data imply that human DCs are able to form podosomes on any adhesion permissive 2-D surface, irrespective of their physico-chemical nature. Interestingly, it has been shown recently that carbon nanotubes, which closely mimic the fibres of the ECM, are able to enhance the physico-chemical stimulation of neurons through a very tight interaction with these cells [52]. It would be of great interest to investigate whether chemical signals presented by nanotubes are differentially integrated by iDCs, thereby influencing podosome formation and organization.

The 2-D spatial arrangement of an adhesive substrate forms a physical stimulus that affects cellular behavior. Lehnert et al. [53] showed that B16 melanoma cells reorganize their FAs at the edge of micropatterned fibronectin spots, demonstrating the importance of signals from spatially rearranged integrin ligands for stable adhesion. We found that DCs can discriminate between adhesive and non-adhesive substrates by selectively forming podosomes on adhesion-permissive areas but not on PEG-coated surfaces. In contrast to FAs [53], podosome formation seems not to depend on integrin stimulation by environmental chemical signals, as DCs also induce podosomes on hydrogels solely coated with a non-specific PLL coating. While mechanisms of ligand-mediated integrin activation have been described in great detail [54], much less is known about physical aspects of integrin activation. However, evidence is emerging that integrins can be directly activated by a mere physical stimulus, such as externally applied strain and shear stress [55, 56]. Our results support this notion and suggest that a physical stimulus, represented by an adhesion-permissive substrate, is sufficient to activate integrins and thereby initiate podosome formation. Intriguingly, as soon as podosome formation is initiated by DCs, a constant number of about 100 podosomes per cell is formed, irrespective of the physico-chemical properties of the microenvironment. This strongly suggests a two-step model in which, on a 2-D surface, podosome formation is initiated by an as yet unknown extracellular physical stimulus, whereas podosome number and maintenance are predominantly controlled by intracellular signaling pathways. Most likely, intracellular components such as actin or other cytoskeletal proteins are limiting the number of podosomes that can be formed per cell.

In an attempt to mimic the 3-D geometry in tissues, efforts have focused on fabricating patterns, topographies, and fibers at the micro- and nanometre scale. This revealed the importance of 3-D substrate geometry in influencing cell behavior [57, 58]. In this study, we found that DCs respond to 3-D micropatterned substrates by rearranging podosomes at sites of high membrane curvature. Remarkably, both an inward and an outward curvature of the plasma membrane were able to direct podosome spatial organization. In addition, changes in surface topography as small as 100 nm could be sensed by the DC and appeared to be sufficient to induce podosome alignment. This

suggests that DCs, when adhering in tissues, might be able to sense individual ECM fibers, which vary in size between 40 and 60 nm, and concentrate podosomes at hotspots of high physical stress. Our data indicate that this occurs irrespectively of the molecular nature of the microenvironment. Moreover, the actin content of podosomes on 3-D substrates was found to be higher than on 2-D surfaces, suggesting that DCs adapt to physical stress by concentrating cytoskeletal components on the edges of 3-D micropatterns. Altogether, our findings render podosomes as extremely suited structures to stabilize cell adhesion in a 3-D microenvironment.

Podosomes predominantly align along the edges of 3-D micropatterns, which are regions of high membrane curvature. Moreover, 3-D geometric cues significantly impair PGE_2-induced RhoA activation, thus preventing podosome dissolution. A model depicting our hypothesis on the geometry-mediated regulation of intracellular signaling is shown in Fig. 5d. Regions of high-membrane curvature selectively concentrate proteins, including BAR domain-containing proteins, and lipids, such as cholesterol, thereby creating signaling platforms at the inner leaflet of the plasma membrane which leads to the directed podosome formation on 3-D micropatterned substrates [42, 59]. Local Rho GTPase activity plays an important role in the regulation of podosomes in DCs [43, 60]. While increased RhoA activity causes podosome dissolution, activation of Cdc42 and Rac1 stimulates podosome formation. Interestingly, many BAR domain-containing proteins either induce hydrolysis or exchange of nucleotides on small G-proteins [61, 62]. In this way, membrane-associated signaling platforms may create a local enrichment of Rho GTPase activity at the plasma membrane, favoring the non-random distribution of podosomes on 3-D micropatterns. More importantly, downstream signals derived from these signaling platforms appear to be propagated through the cytoplasm, since global PGE_2-induced RhoA activation, normally observed on 2-D flat surfaces, is not detectable on 3-D micropatterns. 3-D geometric cues thereby directly influence the cellular signaling pathways that lead to PGE_2-mediated podosome dissolution in human DCs.

We, and others, have demonstrated before that the migratory and immunostimulatory capacity of mature DCs critically depends on the RhoA-mediated dissolution of podosomes [30, 63]. Furthermore, we showed here that, next to the adhesive properties, 3-D micropatterned substrates influence the phagocytic capacity and the maturation status of monocyte-derived iDCs. DC activation is a key process in initiating an effective immune response. It has been shown recently that integrin activity is important in the response of DCs to biomaterials [64]; however, it is still very unclear how different physical and chemical signals influence the activation of DCs. Our results indicate that substrate dimensionality controls many functions associated with DC biology, suggesting that DC activation, and therefore the initiation of an immune response, is critically controlled by the DC microenvironment. How the physical and chemical signals are integrated by the DC to coordinate an immune response remains to be investigated.

Podosomes have been put forward as adhesion structures involved in the matrix degradation and crossing of tissue boundaries [65, 66]. Our studies reveal that podosomes are 3-D geometry-sensing structures potentially acting as cellular stabilizers in a 3-D microenvironment. A major challenge now is to unravel how the cells' geometry-sensing machinery induces podosome alignment and alters the signaling pathways leading to podosome dissolution.

Acknowledgments We thank Dr. C. Mills (IBEC and Nanotechnology platform, Barcelona Science Park, Spain) for help with making the 3-D substrates. We thank Dr. G. Roth (University of Tübingen, Germany) for making the silicon wafer needed to prepare the PDMS stamp. This research was supported by EU grants BIOLIGHT-TOUCH (028781) and Immunanomap (MRTN-CT-2006-035946) and EU-México FONCICYT (C002-2008-1 ALA/127249) awarded to C.G.F. S.v.H. was supported by the Foundation for Fundamental Research on Matter (FOM 01FB06). J.t.R. was supported by NanoNed, the Dutch nanotechnology program of the Ministry of Economic Affairs. A.C. was supported by NWO-Meervoud (836.09.002) and the Human Frontier Science Program (RGY0074/2008). C.G.F. was awarded with a NWO Spinoza prize.

References

1. Orr AW, Helmke BP, Blackman BR, Schwartz MA (2006) Mechanisms of mechanotransduction. Dev Cell 10(1):11–20
2. Thery M, Racine V, Piel M, Pepin A, Dimitrov A, Chen Y, Sibarita JB, Bornens M (2006) Anisotropy of cell adhesive microenvironment governs cell internal organization and orientation of polarity. Proc Natl Acad Sci USA 103(52):19771–19776
3. Engler AJ, Sen S, Sweeney HL, Discher DE (2006) Matrix elasticity directs stem cell lineage specification. Cell 126(4):677–689
4. Fereol S, Fodil R, Laurent VM, Balland M, Louis B, Pelle G, Henon S, Planus E, Isabey D (2009) Prestress and adhesion site dynamics control cell sensitivity to extracellular stiffness. Biophys J 96(5):2009–2022
5. Bershadsky A, Kozlov M, Geiger B (2006) Adhesion-mediated mechanosensitivity: a time to experiment, and a time to theorize. Curr Opin Cell Biol 18(5):472–481
6. Lock JG, Wehrle-Haller B, Stromblad S (2008) Cell-matrix adhesion complexes: master control machinery of cell migration. Semin Cancer Biol 18(1):65–76
7. Delon I, Brown NH (2007) Integrins and the actin cytoskeleton. Curr Opin Cell Biol 19(1):43–50
8. Engler A, Bacakova L, Newman C, Hategan A, Griffin M, Discher D (2004) Substrate compliance versus ligand density in cell on gel responses. Biophys J 86(1 1):617–628

9. Doyle AD, Wang FW, Matsumoto K, Yamada KM (2009) One-dimensional topography underlies three-dimensional fibrillar cell migration. J Cell Biol 184(4):481–490
10. Ahmed I, Ponery AS, Nur EKA, Kamal J, Meshel AS, Sheetz MP, Schindler M, Meiners S (2007) Morphology, cytoskeletal organization, and myosin dynamics of mouse embryonic fibroblasts cultured on nanofibrillar surfaces. Mol Cell Biochem 301(1–2):241–249
11. Ochsner M, Textor M, Vogel V, Smith ML (2010) Dimensionality controls cytoskeleton assembly and metabolism of fibroblast cells in response to rigidity and shape. PLoS One 5(3):e9445
12. Block MR, Badowski C, Millon-Fremillon A, Bouvard D, Bouin AP, Faurobert E, Gerber-Scokaert D, Planus E, Albiges-Rizo C (2008) Podosome-type adhesions and focal adhesions, so alike yet so different. Eur J Cell Biol 87(8–9):491–506
13. Schwartz MA, DeSimone DW (2008) Cell adhesion receptors in mechanotransduction. Curr Opin Cell Biol 20(5):551–556
14. Martinac B (2004) Mechanosensitive ion channels: molecules of mechanotransduction. J Cell Sci 117(12):2449–2460
15. del Rio A, Perez-Jimenez R, Liu R, Roca-Cusachs P, Fernandez JM, Sheetz MP (2009) Stretching single talin rod molecules activates vinculin binding. Science 323(5914):638–641
16. Ren Y, Effler JC, Norstrom M, Luo T, Firtel RA, Iglesias PA, Rock RS, Robinson DN (2009) Mechanosensing through cooperative interactions between myosin II and the actin crosslinker cortexillin I. Curr Biol 19(17):1421–1428
17. Petit V, Thiery JP (2000) Focal adhesions: structure and dynamics. Biol Cell 92(7):477–494
18. David-Pfeuty T, Singer SJ (1980) Altered distributions of the cytoskeletal proteins vinculin and alpha-actinin in cultured fibroblasts transformed by Rous sarcoma virus. Proc Natl Acad Sci USA 77(11):6687–6691
19. Marchisio PC, Cirillo D, Naldini L, Primavera MV, Teti A, Zambonin-Zallone A (1984) Cell-substratum interaction of cultured avian osteoclasts is mediated by specific adhesion structures. J Cell Biol 99(5):1696–1705
20. Tarone G, Cirillo D, Giancotti FG, Comoglio PM, Marchisio PC (1985) Rous sarcoma virus-transformed fibroblasts adhere primarily at discrete protrusions of the ventral membrane called podosomes. Exp Cell Res 159(1):141–157
21. Ochoa GC, Slepnev VI, Neff L, Ringstad N, Takei K, Daniell L, Kim W, Cao H, McNiven M, Baron R, De Camilli P (2000) A functional link between dynamin and the actin cytoskeleton at podosomes. J Cell Biol 150(2):377–389
22. Seals DF, Azucena EF Jr, Pass I, Tesfay L, Gordon R, Woodrow M, Resau JH, Courtneidge SA (2005) The adaptor protein Tks5/Fish is required for podosome formation and function, and for the protease-driven invasion of cancer cells. Cancer Cell 7(2):155–165
23. Buschman MD, Bromann PA, Cejudo-Martin P, Wen F, Pass I, Courtneidge SA (2009) The novel adaptor protein Tks4 (SH3PXD2B) is required for functional podosome formation. Mol Biol Cell 20(5):1302–1311
24. Linder S, Aepfelbacher M (2003) Podosomes: adhesion hot-spots of invasive cells. Trends Cell Biol 13(7):376–385
25. Buccione R, Orth JD, McNiven MA (2004) Foot and mouth: podosomes, invadopodia and circular dorsal ruffles. Nature Rev 5(8):647–657
26. Steinman RM (1991) The dendritic cell system and its role in immunogenicity. Annu Rev Immunol 9:271–296
27. Banchereau J, Steinman RM (1998) Dendritic cells and the control of immunity. Nature 392(6673):245–252
28. van Helden SF, Krooshoop DJ, Broers KC, Raymakers RA, Figdor CG, van Leeuwen FN (2006) A critical role for prostaglandin E_2 in podosome dissolution and induction of high-speed migration during dendritic cell maturation. J Immunol 177(3):1567–1574
29. Burns S, Hardy SJ, Buddle J, Yong KL, Jones GE, Thrasher AJ (2004) Maturation of DC is associated with changes in motile characteristics and adherence. Cell Motil Cytoskeleton 57(2):118–132
30. van Helden SF, van den Dries K, Oud MM, Raymakers RA, Netea MG, van Leeuwen FN, Figdor CG (2010) TLR4-mediated podosome loss discriminates gram-negative from gram-positive bacteria in their capacity to induce dendritic cell migration and maturation. J Immunol 184(3):1280–1291
31. Balaban NQ, Schwarz US, Riveline D, Goichberg P, Tzur G, Sabanay I, Mahalu D, Safran S, Bershadsky A, Addadi L, Geiger B (2001) Force and focal adhesion assembly: a close relationship studied using elastic micropatterned substrates. Nat Cell Biol 3(5):466–472
32. Geiger B, Spatz JP, Bershadsky AD (2009) Environmental sensing through focal adhesions. Natl Rev Mol Cell Biol 10(1):21–33
33. Hirata H, Tatsumi H, Sokabe M (2008) Mechanical forces facilitate actin polymerization at focal adhesions in a zyxin-dependent manner. J Cell Sci 121(17):2795–2804
34. Bershadsky AD, Ballestrem C, Carramusa L, Zilberman Y, Gilquin B, Khochbin S, Alexandrova AY, Verkhovsky AB, Shemesh T, Kozlov MM (2006) Assembly and mechanosensory function of focal adhesions: experiments and models. Eur J Cell Biol 85(3–4):165–173
35. Collin O, Tracqui P, Stephanou A, Usson Y, Clement-Lacroix J, Planus E (2006) Spatiotemporal dynamics of actin-rich adhesion microdomains: influence of substrate flexibility. J Cell Sci 119(9):1914–1925
36. Collin O, Na S, Chowdhury F, Hong M, Shin ME, Wang F, Wang N (2008) Self-organized podosomes are dynamic mechanosensors. Curr Biol 18(17):1288–1294
37. Geblinger D, Geiger B, Addadi L (2009) Surface-induced regulation of podosome organization and dynamics in cultured osteoclasts. Chem Biochem 10(1):158–165
38. Geblinger D, Addadi L, Geiger B (2010) Nano-topography sensing by osteoclasts. J Cell Sci 123(9):1503–1510
39. De Vries IJ, Krooshoop DJ, Scharenborg NM, Lesterhuis WJ, Diepstra JH, Van Muijen GN, Strijk SP, Ruers TJ, Boerman OC, Oyen WJ, Adema GJ, Punt CJ, Figdor CG (2003) Effective migration of antigen-pulsed dendritic cells to lymph nodes in melanoma patients is determined by their maturation state. Cancer Res 63(1):12–17
40. Kusnezow W, Hoheisel JD (2002) Antibody microarrays: promises and problems. BioTechniques Dec 2002 Suppl:14–23
41. Hoff A, Bagu AC, Andre T, Roth G, Wiesmuller KH, Guckel B, Brock R (2010) Peptide microarrays for the profiling of cytotoxic T-lymphocyte activity using minimum numbers of cells. Cancer Immunol Immunother 59(9):1379–1387
42. McMahon HT, Gallop JL (2005) Membrane curvature and mechanisms of dynamic cell membrane remodelling. Nature 438(7068):590–596
43. van Helden SF, Oud MM, Joosten B, Peterse N, Figdor CG, van Leeuwen FN (2008) PGE_2-mediated podosome loss in dendritic cells is dependent on actomyosin contraction downstream of the RhoA–Rho-kinase axis. J Cell Sci 121(7):1096–1106
44. Tsuboi S, Takada H, Hara T, Mochizuki N, Funyu T, Saitoh H, Terayama Y, Yamaya K, Ohyama C, Nonoyama S, Ochs HD (2009) FBP_{17} mediates a common molecular step in the formation of podosomes and phagocytic cups in macrophages. J Biol Chem 284(13):8548–8556
45. Altankov G, Grinnell F, Groth T (1996) Studies on the biocompatibility of materials: fibroblast reorganization of substratum-

bound fibronectin on surfaces varying in wettability. J Biomed Mater Res 30(3):385–391
46. Ozdemir Y, Hasirci N, Serbetci K (2002) Oxygen plasma modification of polyurethane membranes. J Mater Sci Mater Med 13(12):1147–1151
47. Groth T, Altankov G (1996) Studies on cell-biomaterial interaction: role of tyrosine phosphorylation during fibroblast spreading on surfaces varying in wettability. Biomaterials 17(12):1227–1234
48. Dekker A, Reitsma K, Beugeling T, Bantjes A, Feijen J, van Aken WG (1991) Adhesion of endothelial cells and adsorption of serum proteins on gas plasma-treated polytetrafluoroethylene. Biomaterials 12(2):130–138
49. Khang G, Jeon JH, Lee JW, Cho SC, Lee HB (1997) Cell and platelet adhesions on plasma glow discharge-treated poly(lactide-co-glycolide). Biomed Mater Eng 7(6):357–368
50. Chen M, Zamora PO, Som P, Pena LA, Osaki S (2003) Cell attachment and biocompatibility of polytetrafluoroethylene (PTFE) treated with glow-discharge plasma of mixed ammonia and oxygen. J Biomater Sci Polym Ed 14(9):917–935
51. van Kooten TG, Spijker HT, Busscher HJ (2004) Plasma-treated polystyrene surfaces: model surfaces for studying cell-biomaterial interactions. Biomaterials 25(10):1735–1747
52. Cellot G, Cilia E, Cipollone S, Rancic V, Sucapane A, Giordani S, Gambazzi L, Markram H, Grandolfo M, Scaini D, Gelain F, Casalis L, Prato M, Giugliano M, Ballerini L (2009) Carbon nanotubes might improve neuronal performance by favouring electrical shortcuts. Nat Nanotechnol 4(2):126–133
53. Lehnert D, Wehrle-Haller B, David C, Weiland U, Ballestrem C, Imhof BA, Bastmeyer M (2004) Cell behaviour on micropatterned substrata: limits of extracellular matrix geometry for spreading and adhesion. J Cell Sci 117(1):41–52
54. Humphries JD, Byron A, Humphries MJ (2006) Integrin ligands at a glance. J Cell Sci 119(19):3901–3903
55. Katsumi A, Milanini J, Kiosses WB, del Pozo MA, Kaunas R, Chien S, Hahn KM, Schwartz MA (2002) Effects of cell tension on the small GTPase Rac. J Cell Biol 158(1):153–164
56. Tzima E, Kiosses WB, del Pozo MA, Schwartz MA (2003) Localized cdc42 activation, detected using a novel assay, mediates microtubule organizing center positioning in endothelial cells in response to fluid shear stress. J Biol Chem 278(33):31020–31023
57. Fujita S, Ohshima M, Iwata H (2009) Time-lapse observation of cell alignment on nanogrooved patterns. J R Soc Interface 6 Suppl 3:S269–S277
58. Milner KR, Siedlecki CA (2007) Submicron poly(L-lactic acid) pillars affect fibroblast adhesion and proliferation. J Biomed Mater Res A 82(1):80–91
59. Roux A, Cuvelier D, Nassoy P, Prost J, Bassereau P, Goud B (2005) Role of curvature and phase transition in lipid sorting and fission of membrane tubules. EMBO J 24(8):1537–1545
60. Burns S, Thrasher AJ, Blundell MP, Machesky L, Jones GE (2001) Configuration of human dendritic cell cytoskeleton by Rho GTPases, the WAS protein, and differentiation. Blood 98(4):1142–1149
61. Govek EE, Newey SE, Akerman CJ, Cross JR, Van der Veken L, Van Aelst L (2004) The X-linked mental retardation protein oligophrenin-1 is required for dendritic spine morphogenesis. Nat Neurosci 7(4):364–372
62. Salazar MA, Kwiatkowski AV, Pellegrini L, Cestra G, Butler MH, Rossman KL, Serna DM, Sondek J, Gertler FB, De Camilli P (2003) Tuba, a novel protein containing bin/amphiphysin/Rvs and Dbl homology domains, links dynamin to regulation of the actin cytoskeleton. J Biol Chem 278(49):49031–49043
63. Yamakita Y, Matsumura F, Lipscomb MW, Chou PC, Werlen G, Burkhardt JK, Yamashiro S (2011) Fascin1 promotes cell migration of mature dendritic cells. J Immunol 186(5):2850–2859
64. Rogers TH, Babensee JE (2011) The role of integrins in the recognition and response of dendritic cells to biomaterials. Biomaterials 32(5):1270–1279
65. Linder S (2007) The matrix corroded: podosomes and invadopodia in extracellular matrix degradation. Trends Cell Biol 17(3):107–117
66. Gawden-Bone C, Zhou Z, King E, Prescott A, Watts C, Lucocq J (2010) Dendritic cell podosomes are protrusive and invade the extracellular matrix using metalloproteinase MMP-14. J Cell Sci 123(9):1427–1437